

1
2
3
4
5
6
7
8
9
10
11
12

Coupled Feedbacks on the Northern Hemisphere Midlatitude Jet Response to 4xCO₂: Changes in Stratospheric Ozone and the Atlantic Meridional Overturning Circulation

Clara Orbe^{1,2}, David Rind¹, Darryn Waugh³, Jeffrey Jonas^{1,4}, Xiyue Zhang³,
Gabriel Chiodo⁵, Larissa Nazarenko^{1,4}, Gavin Schmidt¹

¹NASA Goddard Institute for Space Studies, New York, NY

²Department of Applied Physics and Applied Mathematics, Columbia University, New York, NY

³Department of Earth and Planetary Sciences, Johns Hopkins University, Baltimore, MD

⁴Center for Climate Systems Research, Earth Institute, Columbia University, New York, NY

⁵1

nstitute for Atmospheric and Climate Science, ETH Zurich, Switzerland

Key Points:

13
14
15
16
17
18
19
20
21
22
23

- The NH midlatitude jet response to 4xCO₂ is modulated by feedbacks from both changes in stratospheric ozone and a weakening of the Atlantic Meridional Overturning Circulation (AMOC).
- Changes in stratospheric ozone affect the NH jet on a “fast” (5-20 year) timescale, during which the jet shifts equatorward. By comparison, a weakening of the AMOC drives a poleward shift in the NH midlatitude jet on “long” (100-150 year) timescales.
- The feedbacks from stratospheric ozone and ocean circulation changes are strongly coupled, since the former drives an equatorward shift of the jet that reduces North Atlantic deep water production through reduced heat fluxes into the ocean, resulting in a stronger decline of the AMOC.

Corresponding author: Clara Orbe, clara.orbe@nasa.gov

24 **Abstract**

25 Ozone, and its response to anthropogenic forcings, provide an important pathway
 26 for the coupling between atmospheric composition and climate. This applies to strato-
 27 spheric ozone as well as ozone in the troposphere; in addition to stratospheric ozone’s
 28 radiative impacts, recent studies have shown that changes in the ozone layer due to $4\times\text{CO}_2$
 29 have a considerable impact on the Northern Hemisphere (NH) tropospheric circulation,
 30 inducing an equatorward shift of the North Atlantic jet during boreal winter. Here we
 31 show that this equatorward jet shift induces a more rapid weakening of the Atlantic Merid-
 32 ional Overturning Circulation (AMOC), resulting in a poleward shift of the jet on longer
 33 timescales. As such, feedbacks from both stratospheric ozone and the AMOC result in
 34 a two-timescale response of the NH midlatitude jet in response to $4\times\text{CO}_2$: a “fast” re-
 35 sponse (5-20 years) during which the North Atlantic jet shifts equatorward and a “long”
 36 response (~ 100 -150 years) during which the jet shifts poleward. The latter is driven by
 37 a weakening of the AMOC that develops in response to weaker surface zonal winds, that
 38 result in reduced heat fluxes out of the subpolar gyre, reducing North Atlantic deep wa-
 39 ter formation. Our results suggest that stratospheric ozone changes in the tropical lower
 40 stratosphere can have a surprisingly powerful effect on the AMOC, independent of other
 41 aspects of climate change.

42 **Plain Language Summary**

43 **1 Introduction**

44 There is large uncertainty in the atmospheric circulation response to increasing green-
 45 house gases (e.g., Shepherd (2014)). Although models generally predict a poleward shift
 46 of the westerly jet, the magnitude of this shift is highly uncertain (e.g., Vallis et al. (2015);
 47 Grise and Polvani (2014)) as are its underlying drivers (T. A. Shaw (2019)). This is es-
 48 pecially true in the Northern Hemisphere (NH), where there are opposing thermodynamic
 49 influences, i.e. opposite meridional temperature gradient responses at the surface ver-
 50 sus the upper troposphere (T. Shaw et al. (2016)). Thus, while enhanced warming in the
 51 lower polar troposphere relative to the lower tropical troposphere (i.e., Arctic amplifi-
 52 cation) contributes to reduced meridional temperature gradients, increases in upper tro-
 53 pospheric tropical warming contribute to enhanced temperature gradients aloft (Butler
 54 et al. (2010); Yuval and Kaspi (2020)) and it is not clear how these competing processes
 55 affect the zonal mean jet.

56 Many processes have been shown to influence the response of meridional temper-
 57 ature gradients to increased CO_2 , including polar amplification (see Smith et al. (2019)
 58 and references therein) and cloud feedbacks (e.g., Ceppi and Hartmann (2015); Voigt and
 59 Shaw (2015)). By comparison, composition feedbacks associated with the ozone response
 60 to CO_2 have been less well examined although stratospheric ozone changes have been
 61 identified as an important pathway coupling composition to climate (Isaksen et al. (2009)).
 62 In particular, the stratospheric ozone response to $4\times\text{CO}_2$ consists of robust decreases in
 63 the tropical lower stratosphere (LS), increases in the tropical upper stratosphere and in-
 64 creases over high latitudes (Chiodo et al., 2018). While the exact details of these changes
 65 are model dependent, especially over high latitudes, the general pattern is very consis-
 66 tent among models (Nowack et al. (2015), Chiodo et al. (2018), Chiodo and Polvani (2019)
 67 (hereafter CP2019)).

68 This pattern of reduced (increased) ozone over the tropical lower (high latitude)
 69 LS in response to $4\times\text{CO}_2$ has immediate implications for temperature gradients in the
 70 stratosphere by cooling the tropics and warming high latitudes (Nowack et al. (2015);
 71 Chiodo et al. (2018)). As CP2019 showed, these changes in temperature gradients drive
 72 an anomalous equatorward shift of the midlatitude jet, not only in the Southern Hemi-
 73 sphere (SH), but also in the Northern Hemisphere (NH), where anomalies extend down

74 into the lower troposphere and are concentrated over the Atlantic, resembling the neg-
75 ative phase of the North Atlantic Oscillation (NAO). Thus, in contrast to the ozone feed-
76 back on equilibrium climate sensitivity (Nowack et al. (2015)), which has been shown
77 to be model dependent (Marsh et al. (2016)), the ozone feedback on temperature gra-
78 dients is robust.

79 A more recent study by Zhang et al. (Submitted), that considered two models that
80 differed only in their representation of interactive chemistry, also showed that changes
81 in composition can impact the sign of the NH midlatitude jet response to increased CO₂.
82 However, in contrast to CP2019, the long-term impact of this compositional feedback
83 was a poleward, not equatorward, shift in the North Atlantic jet. This poleward shift
84 of the jet was linked to changes in the ocean circulation, with the authors noting that
85 the AMOC featured a stronger decline in the interactive versions of simulations in which
86 trace gases and aerosols were allowed to respond to CO₂, relative to non-interactive sim-
87 ulations. Indeed, recent studies have highlighted the large influence that changes in the
88 AMOC exert on the response of the NH midlatitude jet to increased CO₂ (Gervais et
89 al. (2019)). Specifically, models featuring a larger AMOC decline also tend to produce
90 a stronger poleward jet shift (Bellomo et al. (2021); Liu et al. (2020); Orbe et al. (Un-
91 der Review)).

92 While Zhang et al. (Submitted) linked a stronger NH poleward jet shift to a more
93 pronounced AMOC decline, they did not examine the processes by which interactive chem-
94 istry affected the ocean circulation. At the same time, it is well known from the oceanog-
95 raphic literature that variations in the jet – namely those resembling the NAO – can
96 influence variability of the Atlantic Meridional Overturning Circulation (AMOC) through
97 changes in wind stress (Marshall et al. (2001); Zhai and Marshall (2014)). Modified air-
98 sea fluxes of heat, water and momentum associated with variations in the NAO alter ver-
99 tical and horizontal density gradients in the subpolar gyre, inducing changes in deep wa-
100 ter formation and the AMOC (e.g., Visbeck et al. (1998); Delworth and Dixon (2000)).
101 This pathway via the NAO has been used to demonstrate how sudden stratospheric warm-
102 ings influence the variability of heat flux anomalies into the ocean and ocean mixed layer
103 depths in the North Atlantic (O’Callaghan and Mitchell (2014)) as well as the strength
104 of the AMOC itself (Reichler et al. (2012)).

105 To this end, here we hypothesize that the ozone-induced negative NAO wind anoma-
106 lies reported in CP2019 provide a potential pathway through which stratospheric ozone
107 changes influence the AMOC. Since both ozone changes and the AMOC influence the
108 NH jet (in the opposite sense), these pathways comprise a coupled atmosphere-ocean feed-
109 back on the NH midlatitude jet response to increased CO₂. We begin by showing results
110 from global warming experiments produced with the new high-top coupled atmosphere
111 ocean version of the NASA Goddard Institute for Space Studies (GISS) climate model
112 that were submitted to the Coupled Model Intercomparison Project Phase 6 (CMIP6)
113 (Eyring et al. (2016)).

114 Previous studies have long shown that interactive atmospheric composition can strongly
115 influence the AMOC, placing an almost exclusive focus on the role of aerosols (Booth
116 et al., 2012; Cowan & Cai, 2013; Swingedouw et al., 2015). More recently, Rind et al.
117 (2018) also identified a larger sensitivity of the AMOC response to global warming us-
118 ing an interactive configuration of the CMIP5 version of the GISS climate model (GISS-
119 E2-R), compared to a non-interactive version. In that study, multicentennial cessations
120 of the AMOC were found to occur in association with reduced evaporation relative to
121 precipitation over local regions of cooler SSTs, with natural aerosols (primarily sea salt)
122 acting to enhance this surface cooling. Changes in internal ocean freshwater transports,
123 by comparison, were shown to play a less important role in initiating changes in the AMOC,
124 relative to this indirect affect of aerosols on cloud cover through cooling of sea surface
125 temperatures.

As in Rind et al. (2018) here we show that compositional feedbacks play an important role on the response of the AMOC to CO₂ via their influence on surface fluxes and surface temperatures. However, in contrast to the previous studies, we show that the AMOC response is largely associated with changes in stratospheric ozone, not aerosols, using new experiments in which the stratospheric ozone response to 4xCO₂ is isolated from changes in other trace gases and aerosols. As we show, our model captures the ozone-induced negative NAO-like pattern first reported in CP2019. In addition, however, our model also shows that this ozone-driven change in surface friction speed further weakens the AMOC, resulting in a long-term poleward shift of the NH jet. As a result, we find that the ozone feedback on the NH circulation depends on the response of the ocean circulation. That is, our results suggest that ozone modulates the NH jet response to CO₂ via two distinct timescales: a “fast” response favoring an equatorward jet shift and a “long” response favoring a poleward jet shift. While the former was documented in CP2019, the latter has, to the best of knowledge, not been reported in previous studies.

We begin by discussing methods in Section 2 and present key results and conclusions in Sections 3 and 4, respectively.

2 Methods

2.1 Model and Configurations

Here we use the NASA Goddard Institute for Space Studies (GISS) “Middle Atmosphere (MA)” Model E2.2 (Rind et al. (2020); Orbe et al. (2020)). E2.2 consists of 102 vertical levels spanning the surface up to 0.002 hPa and is run at a horizontal resolution of 2 degrees by 2.5 degrees. Orographic and non-orographic gravity wave drag is parameterized following Lindzen (1987) and Rind et al. (1988), producing in E2.2 a quasibiennial oscillation (QBO) that compares well with observations as well as improved stratospheric polar vortex variability (Ayarzagüena et al. (2020); Rind et al. (2020)). Among the different model versions discussed in Rind et al. (2020) here we focus on the “Altered-Physics” (-AP) Version (E2.2-AP) because this is the configuration that was submitted CMIP6 and presented in recent studies (Ayarzagüena et al. (2020); DallaSanta et al. (2021a, 2021b)).

We begin by showing the results reported in Zhang et al. (Submitted) using both “Non-INTERactive” (NINT) (Table 1, row 1-3) and fully interactive OMA (“One-Moment Aerosols”; Bauer et al. (2020)) configurations (Table 1, row 4-6). In the NINT configuration (denoted in CMIP6 as “physics version 1” on the Earth System Grid Federation (ESGF; <https://esgf.llnl.gov>)) all trace gases and aerosols are set to preindustrial values. Hence, in the 2- and 4xCO₂ NINT runs neither ozone nor other trace gases (besides water vapor) change in response to increased CO₂. By comparison, the OMA 2- and 4xCO₂ runs (denoted in CMIP6 as “physics version 3” on ESGF) capture the full nonlinear ozone response to CO₂, as well as composition feedbacks associated with other trace gases and aerosols.

In order to isolate the role of ozone feedbacks on the circulations, we then use a linearized ozone (LINOZ) configuration (Table 1, row 7-8). In LINOZ (McLinden et al. (2000)) the ozone field is calculated interactively by Taylor expanding the equation of state around present-day (2000–2010) values such that the ozone tendency is, to first-order, parameterized as a function of the local ozone mixing ratio, temperature, and overhead column ozone. Tropospheric ozone is calculated using monthly mean ozone production and loss rates archived from GEOS-CHEM (Rind et al. (2014)). In contrast to NINT, therefore, the LINOZ ensemble captures the influence of the ozone response to CO₂ on the large-scale circulation. Unlike OMA, however, it is much more computationally efficient to run and isolates the ozone feedback from feedbacks related to other trace gases and aerosols. DallaSanta et al. (2021a) previously showed that the LINOZ ozone

Table 1. The Model E2.2 experiments presented in this study, including preindustrial control, abrupt 2xCO₂ and abrupt 4xCO₂ simulations using both NINT (rows 1-3) and OMA (rows 4-6) configurations. Four NINT abrupt 4xCO₂ ensemble members are included (row 3) in order to compare with a four member 4xCO₂ ensemble produced using the LINOZ configuration (row 8). The 4xCO₂ ensemble mean LINOZ ozone response is also used to force an AMIP preindustrial experiment (row 9) in which all forcings other than ozone are set to preindustrial values. A LINOZ preindustrial control simulation (row 7) is also examined. All coupled simulations are run using the the GISS Ocean v1 (GO1) (i.e., “-G” in CMIP6 notation).

Configuration	Ozone	CO ₂	Ensemble Size	SSTs and SICs
NINT	Preindustrial	Preindustrial	1	coupled (-G ocean)
NINT	Preindustrial	2xCO ₂	1	coupled (-G ocean)
NINT	Preindustrial	4xCO ₂	4	coupled (-G ocean)
OMA	Preindustrial	Preindustrial	1	coupled (-G ocean)
OMA	2xCO ₂	2xCO ₂	1	coupled (-G ocean)
OMA	4xCO ₂	4xCO ₂	1	coupled (-G ocean)
LINOZ	Preindustrial	Preindustrial	1	coupled (-G ocean)
LINOZ	4xCO ₂	4xCO ₂	4	coupled (-G ocean)
NINT	LINOZ 4xCO ₂	Preindustrial	4	AMIP (PiControl SSTs and SICs)

176 parameterization reproduces well the vertical structure and seasonal cycle of stratospheric
 177 ozone obtained from the fully interactive OMA configuration (see their Figure 1).

178 2.2 Experiments

179 For the different model configurations (NINT, OMA, LINOZ) we perform 150-year-
 180 long abrupt 2- and 4xCO₂ experiments, in which CO₂ values are abruptly doubled and
 181 quadrupled relative to preindustrial values. For each model configuration, these exper-
 182 iments are branched from a corresponding preindustrial control simulation. For NINT
 183 and LINOZ four-member 4xCO₂ ensembles are run in order to assess the robustness of
 184 any ozone feedbacks. These experiments are all conducted using the coupled-atmosphere-
 185 ocean version of E2.2-AP coupled to the GISS Ocean v1 (GO1) (i.e., “-G” in CMIP6 no-
 186 tation, hereafter simply E2-2-G). For coupled atmosphere-ocean configurations in which
 187 (four-member) ensembles are run, different ensemble members are chosen from differ-
 188 ent initial ocean states spaced 20 years apart in the corresponding preindustrial control
 189 simulation.

190 In addition to the coupled atmosphere-ocean experiments, we also present results
 191 from a four-member ensemble of 60-year-long atmosphere-only AMIP experiments in which
 192 sea surface temperatures (SSTs) and sea ice concentrations (SICs) are fixed to preindus-
 193 trial values, but the monthly mean time-evolving ensemble mean ozone response from
 194 the coupled LINOZ 4xCO₂ experiments is prescribed (Table 1, row 9). This allows us
 195 to quantify the impact of the ozone feedback represented in LINOZ on the large-scale
 196 circulation, absent any contributions from changes in background CO₂, sea ice concen-
 197 trations or sea surface temperatures.

198

2.3 Analysis

199

2.3.1 Timescales

200

201

202

203

204

205

206

207

When examining the midlatitude jet response to increased CO₂ we account for the fact that extratropical circulation changes consist of distinct “fast” and “slow” responses (Ceppi et al. (2018), hereafter CZS2018). More precisely, CZS2018 show that most of the shift of the midlatitude jets occurs within 5-10 years of a steplike (abrupt) CO₂ forcing, with little shifts occurring during a slower response over which SSTs change over subsequent decades. In contrast to the Southern Hemisphere, zonal asymmetries play an important role in the Northern Hemisphere, where the influence of local patterns in sea surface temperature change can result in oppositely signed jet shifts on “slow” timescales.

208

209

210

211

212

213

Given the potential for compensating jet shifts occurring on distinct timescales, we decompose the CO₂ circulation response into “fast” and “long” timescale responses. This consideration is especially important as it relates to our hypothesis that stratospheric ozone changes can first result in an initial equatorward shift of the jet (CP2019) but, over time, result in a poleward shift of the jet via their influence on the AMOC (Bellomo et al., 2021; Orbe et al., Under Review).

214

215

216

217

218

219

220

221

222

223

224

225

226

227

228

229

In order to account for the large internal variability in our runs, perhaps related to a somewhat larger ENSO amplitude in our model compared to observations (Rind et al. (2020)), we modify the original approach used in CZS2018 to define our “fast” response as the difference between the ensemble mean 4xCO₂ response, averaged over years 5-20 (as opposed to years 5-10), and the corresponding preindustrial control simulation. In addition, instead of focusing on the “slow” response, defined in that study as the difference between averages over years 120-140 and years 5-10, here we examine the “long” response, defined as the difference between the ensemble mean 4xCO₂ response, averaged over years 100-150, and the preindustrial control simulation. While this definition departs from the approach used in CZS2018, it is more consistent with the Zhang et al. (Submitted) and CP2019 studies motivating our study, with which we directly compare our results throughout. Note that in response to an abrupt quadrupling of CO₂ the NINT model configuration produces global mean surface temperature “fast” and “long” responses of ~2.9°C and ~3.9°C, respectively. Statistical significance of all changes are assessed relative to the interannual variability in the corresponding preindustrial control simulation for each configuration (Table 1, rows 1,4,7).

230

2.3.2 Analysis Fields

231

232

233

234

235

236

237

238

239

240

241

242

243

244

In addition to the atmospheric variables examined in CP2019 (i.e., zonal mean wind, zonal mean temperature, surface temperature, 850 hPa zonal wind) we examine ocean variables relevant to understanding the evolution of the AMOC and its coupling to the atmosphere. In particular, in addition to examining the surface mixed layer depths we also examine sea surface temperatures, surface friction speed, horizontal ocean heat and salinity transports as well as the net heat fluxes which, together with the net freshwater fluxes, F (inferred from precipitation minus evaporation (P-E)), provide information about the surface buoyancy forcing (Large and Yeager (2009)). In our simulations, the preindustrial climatological buoyancy forcing over the North Atlantic is dominated by the net heat fluxes ($Q = Q_H + Q_E + Q_S + Q_L$), which are defined to be positive into the ocean (Appendix Figure 1, left). These are further partitioned into their respective latent heat (Q_E) and sensible heat (Q_H) contributions as we find that the net solar (Q_S) and longwave (Q_L) flux radiative contributions are negligible over the North Atlantic region (Appendix Figure 1, right).

245

246

Given our interest in the Northern Hemisphere we focus primarily on December-January-February (DJF). The ocean heat transport changes in our simulations are also

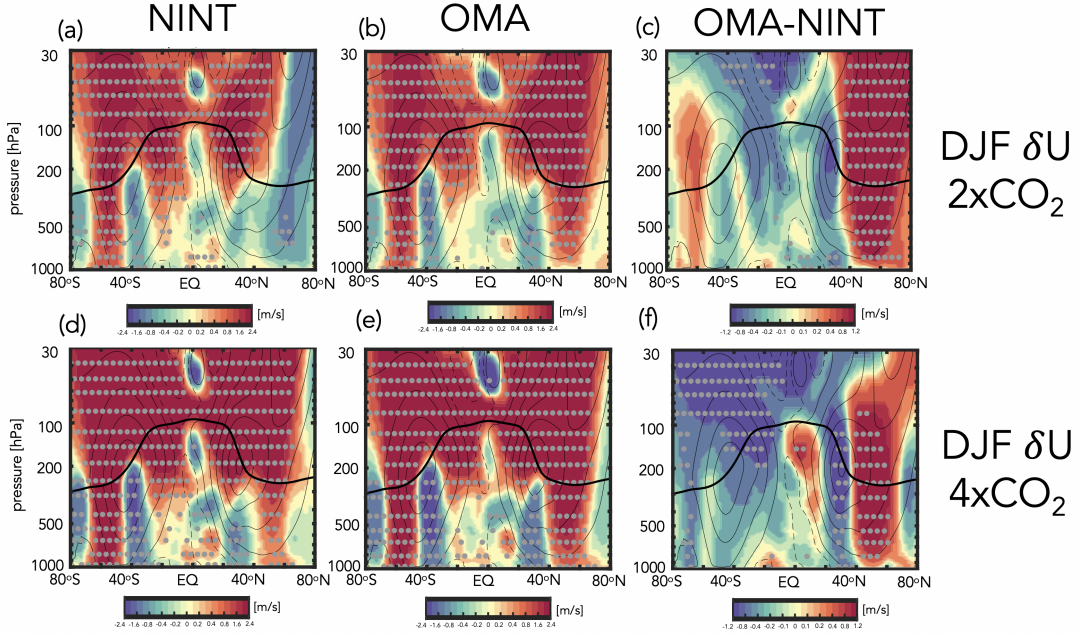


Figure 1. Colors show the December-January-February (DJF) response of the zonal mean zonal winds, U , to an abrupt doubling (top) and quadrupling (bottom) of CO_2 , averaged over years 100-150. Results are shown for the “Non-INTeractive” (NINT) (a,d) and fully interactive OMA (“One-Moment Aerosols”) configurations (b,e), where one ensemble member has been used for each forcing scenario. The OMA - NINT differences are also shown (c,f). Black contours denote climatological mean DJF U values (contour interval: 8 m/s). Stippled regions are statistically significant and the black thick line shows the climatological mean tropopause in the preindustrial control NINT simulation. Note that all colorbar bounds are consistent with those used in Chiodo and Polvani (2019) in order to facilitate comparisons with that study.

247 most pronounced during DJF, consistent with the analyses presented in Romanou et al.
 248 (Under Review) and Orbe et al. (Under Review).

249 **3 Results**

250 **3.1 Abrupt $2x\text{CO}_2$ and $4x\text{CO}_2$ Zonal Mean Wind Response: OMA versus NINT**
 251

252 Before focusing on ozone feedbacks, we first review the OMA versus NINT differ-
 253 ences in NH jet behavior that were presented in Zhang et al. (Submitted) (Figure 1). In
 254 the stratosphere the zonally averaged DJF wind response to 2- and $4x\text{CO}_2$ features an
 255 acceleration at nearly all latitudes, consistent with amplified warming in the tropical upper
 256 troposphere (T. A. Shaw (2019)) and increased cooling of the stratosphere with height
 257 (Garcia and Randel (2008)). Similar wind responses emerge in both the NINT and OMA
 258 configurations, except over northern high latitudes at $2x\text{CO}_2$, where the differences in
 259 NINT are not statistically significant.

260 In the troposphere, however, there are noticeable differences between the OMA and
 261 NINT simulations. In particular, the NH midlatitude jet features a much stronger pole-
 262 ward shift in OMA, compared to NINT (Figures 3 and 6 in Zhang et al. (Submitted) for
 263 comparison). As discussed in that study, the stronger response in OMA results in en-

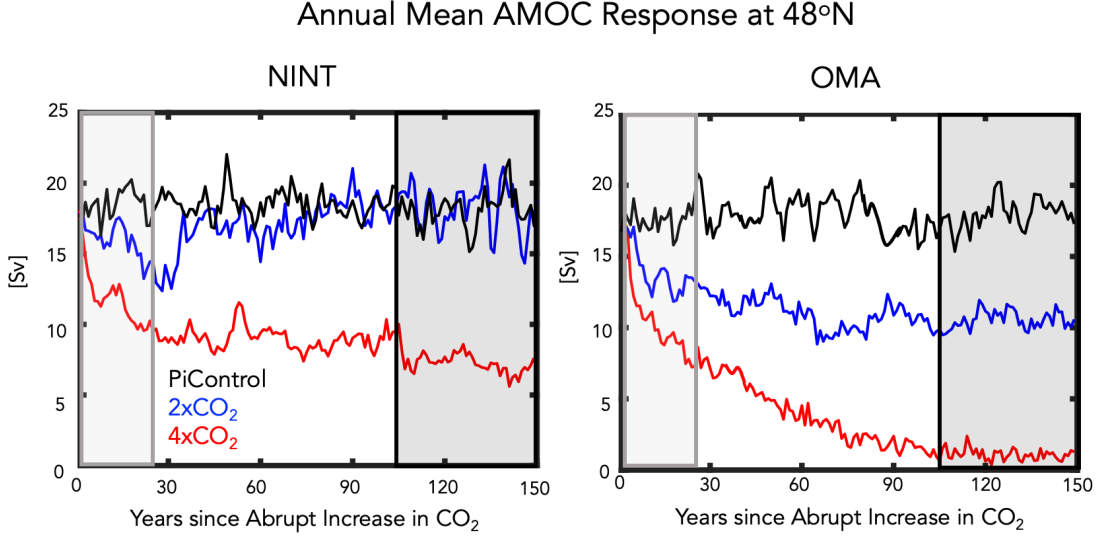


Figure 2. Changes in the annual mean maximum overturning stream function in the Atlantic ocean, evaluated 48°N, for the preindustrial control (black), abrupt 2xCO₂ (blue) and abrupt 4xCO₂ (red) simulations. Results for the NINT (left) and OMA (right) configurations are shown. Black and grey shaded boxes denote the “fast” and “long” timescale response averaging periods.

264 hanced eddy mixing along isentropes on the poleward flank of the NH jet, resulting in
 265 increased transport of tracers from the northern midlatitude surface to the Arctic (not
 266 shown). This difference between OMA and NINT occurs at both 2- and at 4xCO₂, re-
 267 sulting in a nonlinearity in the jet (and tracer transport) response in NINT that is not
 268 present in the OMA simulations. In the SH, by comparison, the differences between OMA
 269 and NINT are much smaller and not statistically significant.

270 Zhang et al. (Submitted) showed that the nonlinearity in NH jet behavior evident
 271 in the “long” response in the NINT model configuration was related to a nonlinear AMOC
 272 response to CO₂ forcing (Figure 2). That is, despite an initial weakening, in response
 273 to 2xCO₂, the AMOC eventually recovers in the NINT 2xCO₂ simulation to preindus-
 274 trial values, in contrast to the response to 4xCO₂ in which the AMOC is about 10 SV
 275 weaker than the preindustrial control (black boxes). This results in a so-called “AMOC
 276 nonlinearity” of ~5SV in the NINT configuration. By comparison, in the OMA config-
 277 uration, the AMOC weakens by ~7 and ~17 SV in the 2- and 4xCO₂ simulations, re-
 278 spectively, representing only a very weak nonlinearity in the AMOC (of ~1.5 SV).

279 As it is difficult to meaningfully interpret the zonal mean wind response in the NH,
 280 where there are large zonal variations in the midlatitude jet (Simpson et al. (2014)), we
 281 next compare the 850 hPa zonal wind changes between the NINT and OMA 4xCO₂ sim-
 282 ulations, further distinguishing between “fast” and “long” responses (Figure 3). We be-
 283 gin with the NINT equilibrated or “long” response (i.e. years 100-150), which consists
 284 of a poleward jet shift over the Pacific basin and an acceleration and eastward extension
 285 of the jet over the Atlantic (Fig. 3b). This pattern is amplified in the OMA run (Fig.
 286 3d), in which both the strengthening of the jet over the Atlantic and its poleward shift
 287 over the Pacific are more pronounced. This wind response in OMA, relative to NINT,
 288 is consistent with the jet differences identified in Orbe et al. (Under Review) between
 289 two non-interactive simulations of the GISS low-top climate model in which only the AMOC
 290 strength differed. This suggests that the jet differences between OMA and NINT on these

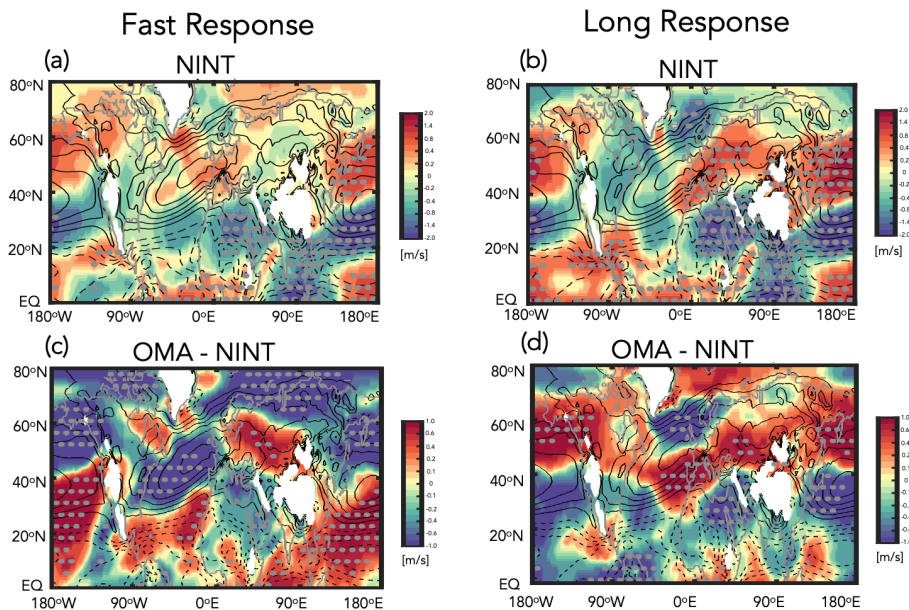
DJF 4xCO₂ δU at 850 hPa

Figure 3. Colors show 4xCO₂ (four member) ensemble mean change in the DJF 850 hPa zonal winds for the NINT configuration, decomposed into “fast” (i.e. years 5-20) (a) and “long” (i.e. years 100-150) (b) responses. The OMA - NINT fast and long differences are shown in (c) and (d), respectively. Note that one ensemble member is used in displaying the OMA - NINT differences. Black contours denote climatological mean DJF values (U contour interval: 2 m/s) and stippled regions are statistically significant.

291 longer timescales are primarily driven by differences in the AMOC response, as concluded
 292 in Zhang et al. (Submitted).

293 Figure 2 (grey boxes) highlights how the AMOC differences between OMA and NINT
 294 noted in Zhang et al. (Submitted) arise very early in the simulations (within the first 20
 295 years). Over these years – which comprise the “fast” response – the impact of interac-
 296 tive chemistry on the zonal wind changes is very different (Fig. 3a,c). In particular, over
 297 the Atlantic, interactive composition results in a strong weakening over the jet core and
 298 an acceleration on the equatorward flank of the jet (Fig. 3c). The jet response is also
 299 very different over the Pacific, where the jet shifts equatorward, not poleward as in the
 300 NINT simulation (Fig. 3a).

301 This fast composition feedback that occurs over years 5-20 is consistent with the
 302 results from CP2019, who showed that the ozone response to 4xCO₂ induces a weaken-
 303 ing of the North Atlantic jet and a strengthening on its equatorward flank (see their Fig-
 304 ure 6). This response is reminiscent of the negative phase of the NAO which previous
 305 studies have shown can result in a weaker AMOC Delworth and Zeng (2016). In CP2019,
 306 however, this response is realized through changes in stratospheric ozone alone, whereas
 307 in OMA all trace gases and aerosols are responding. Furthermore, the significance of this
 308 rapid response with only one ensemble member is uncertain, particularly during the first
 309 5-20 years when the signal is confounded by large internal variability. To this end, next
 310 we present results from the larger (4-member) LINOZ ensemble to examine whether the
 311 fast response in the NH jet is related to stratospheric ozone changes.

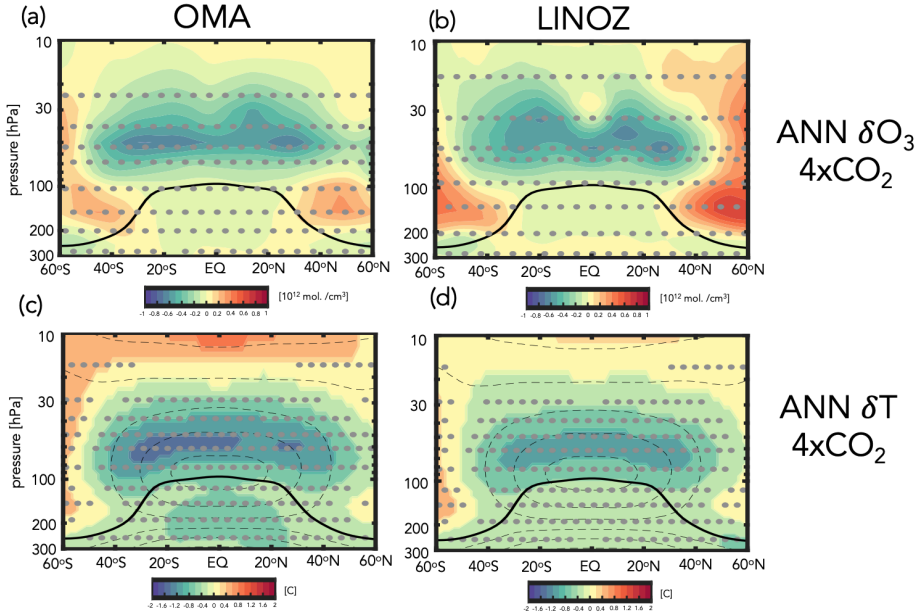


Figure 4. Colors show the annual averaged change in ozone number density (top) and temperature (bottom) in response to $4xCO_2$. Results for OMA (left) and LINOZ (right) are shown, averaged over years 5-20. One simulation is shown for OMA and the four-member ensemble mean response is shown for LINOZ. Black contours in the bottom panels show climatological mean temperatures (contour interval: 10 C). Stippled regions are statistically significant and the black thick line shows the climatological mean tropopause in the preindustrial control NINT simulation.

312
313

3.2 Abrupt $4xCO_2$ Stratospheric Ozone and Temperature Responses: OMA versus LINOZ

314
315
316
317
318
319
320
321
322

Before examining the circulation response in the LINOZ ensemble, we first compare the annually averaged ensemble mean LINOZ $4xCO_2$ ozone response with that from the OMA simulation (Figure 4). The amplitude and pattern of the ozone response in the LINOZ ensemble (Fig. 4b) is generally very similar to the ozone response in the OMA simulation (Fig. 4a). In both configurations the pattern of the $4xCO_2$ changes reflects a decrease in tropical LS ozone, associated with enhanced tropical upwelling (Garcia and Randel (2008)), and enhanced concentrations over high latitudes. Over all latitudes the ozone changes are statistically significant, relative to interannual variability in the preindustrial control simulation.

323
324
325
326
327
328
329
330

Over northern high latitudes there are some differences in the mid-to-lower stratosphere ($\sim 30-100$ hPa) between LINOZ and OMA, generally consistent with Chiodo et al. (2018), who found that in this region the ozone response to CO_2 is somewhat more model dependent. Furthermore, both simulations feature small changes in the troposphere. Overall, therefore, the LINOZ scheme captures the gross characteristics of the ozone abrupt $4xCO_2$ response expected from previous studies. Note that this ozone response occurs in both simulations within the 5-20 years that comprise the “fast” response timescale, although full equilibration at high latitudes does take somewhat longer (not shown).

331
332
333

In response to the ozone changes to $4xCO_2$ both the OMA simulation and LINOZ ensemble produce cooling in the tropical lower stratosphere and warming over high latitudes (Fig. 4c,d). The amplitude of the cooling is $\sim 3K$ in the tropical lower stratosphere,

334 and is more-or-less collocated with the region of largest ozone decreases. Further anal-
 335 ysis of the temperature tendencies reveals that in our model the cooler temperatures in
 336 the tropics (20°S-20°N) and high latitudes (40°N) are respectively associated with re-
 337 duced and increased radiative heating, primarily in the shortwave component (not shown).
 338 Dynamically, comparisons of the 4xCO₂ changes in the residual mean stream function
 339 show a weaker response in LINOZ, relative to NINT (Appendix Figure 2). This ozone
 340 feedback on the Brewer-Dobson circulation, first identified in (DallaSanta et al., 2021a),
 341 would contribute to reduced upwelling (and adiabatic cooling) and ozone transport within
 342 the lower tropical stratosphere. These circulation changes are therefore not the primary
 343 drivers of the temperature response which, rather, is primarily determined by the short-
 344 wave radiative response to ozone changes.

345 Despite the somewhat stronger cooling in OMA (Fig. 4c) compared to NINT (Fig.
 346 4d), the temperature response in both configurations is within the 2-4 K range documented
 347 in CP2019 (note that all colorbars used are consistent with that study to facilitate com-
 348 parisons with their results). As the authors of that study emphasized, the temperature
 349 changes due to ozone are of a similar magnitude to the temperature changes due to 4xCO₂
 350 alone in the tropical lower stratosphere (i.e., considering no ozone feedback), where the
 351 stratosphere cools by ~2K in the NINT ensemble (not shown). The ozone changes present
 352 in LINOZ (and OMA) therefore represent a substantial feedback on the CO₂-induced
 353 cooling in the stratosphere.

354 3.3 Ozone Feedback on Northern Hemisphere Jet: Fast Response

355 The temperature response due to ozone is dynamically consequential for the tropo-
 356 sphere to the extent that it modifies temperature gradients (and winds) in the lower
 357 stratosphere. Indeed, the LINOZ ensemble shows a strong enhancement of lower strato-
 358 spheric temperature gradients in both hemispheres on both the fast and long response
 359 timescales (Fig. 5a,b). In the fast response, which we focus on first, this reduction in the
 360 meridional temperature gradient near the tropopause has important consequences for
 361 the midlatitude jet in both hemispheres, which strengthens above and along the jet core
 362 and weakens on the poleward flank of the jet over latitudes north of ~50°N (Fig. 5c).
 363 The winds also accelerate equatorward of the jet core, relative to NINT, in both hemi-
 364 spheres, although the response is only statistically significant in our model in the NH.
 365 This ozone-induced response in the jet is very similar to the pattern of the wind response
 366 reported in CP2019 (see their Figures 4 and 5). As with the temperature changes oc-
 367 ccurring in the lower stratosphere, the wind response to ozone changes is similar in mag-
 368 nitude to the 4xCO₂ response, again suggesting a substantial modulation of the circula-
 369 tion in both hemispheres by ozone changes alone.

370 The fast zonal mean response to ozone changes reflects a weakening of the polar
 371 jet over all longitudes, with the largest negative anomalies concentrated over the Atlantic
 372 ocean that are flanked equatorward by positive wind anomalies (Fig. 6a). These wind
 373 changes are vertically coherent throughout the troposphere as the LINOZ-NINT changes
 374 are similar at 300 hPa (not shown). This LINOZ-NINT wind dipole over the Atlantic
 375 is very similar to the fast wind response captured in the fully interactive OMA simula-
 376 tion (Fig. 3c), especially over the Atlantic. Over the Pacific, by comparison, the OMA
 377 and LINOZ responses are different, consistent with CP2019 who found no robust ozone
 378 feedback over the Pacific (see their Figure 5). Furthermore, the weakening of the North
 379 Atlantic jet in the LINOZ simulations is associated with warming over North America
 380 and cooling over the North Atlantic and over Eurasia, resembling the negative phase of
 381 the NAO (Fig. 6c). A similar surface temperature anomaly was identified in CP2019 (see
 382 their Figure 7) in conjunction with positive sea level pressure (SLP) anomalies over the
 383 Arctic, both features being reminiscent of a negative NAO (Appendix Figure 3, top).

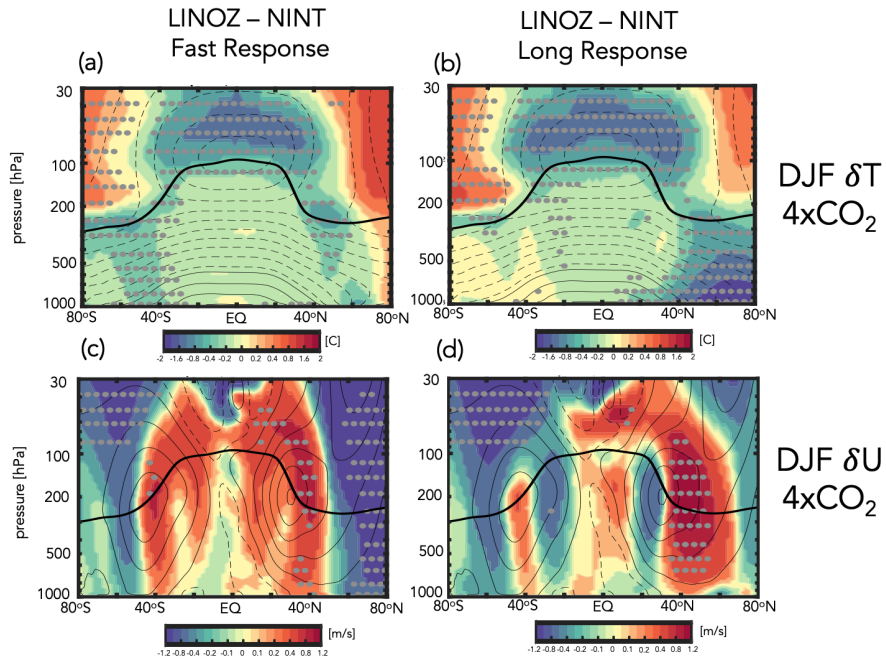


Figure 5. Colors show the LINOZ-NINT ensemble mean difference in the DJF response of the zonal mean temperatures, T (top) and zonal winds, U (bottom) in response to an abrupt quadrupling of CO_2 . Both LINOZ and NINT ensembles consist of four members. Responses are decomposed into “fast” (a,c) and “long” (b,d) changes. Contours denote climatological mean DJF values (T contour interval: 10 C; U contour interval: 8 m/s). Stippled regions are statistically significant and the black thick line shows the climatological mean tropopause in the preindustrial control simulation.

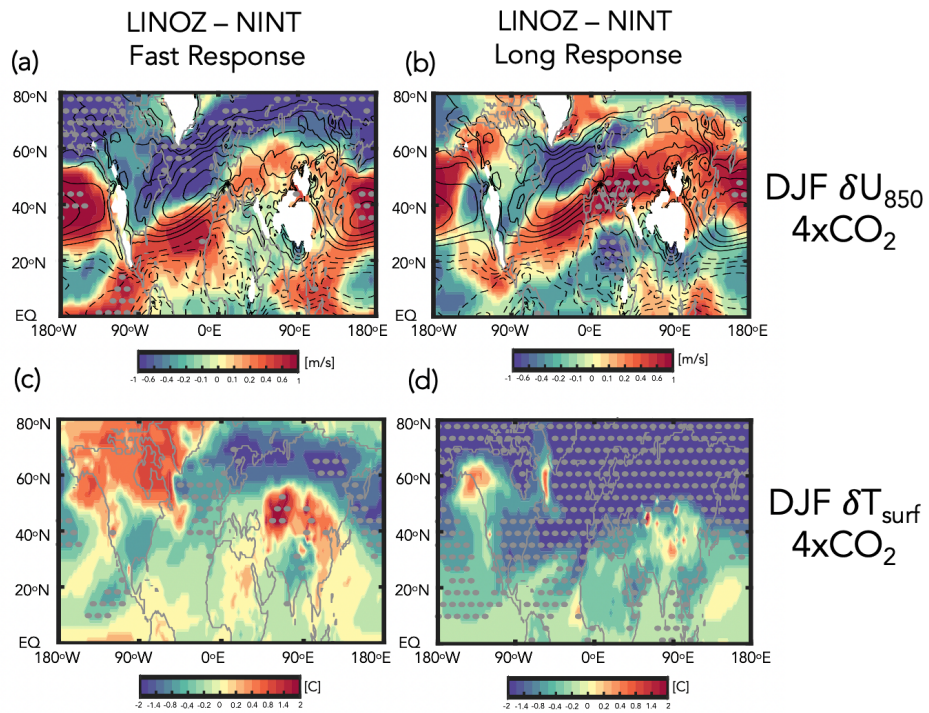


Figure 6. Same as Figure 5, except showing the LINOZ-NINT DJF response in the 850 hPa zonal winds (top) and surface temperatures (bottom). Contours in top panels denote climatological mean DJF values of U_{850} (contour interval: 2 m/s). Note the similarity between the “fast” wind response shown in (a) and the CP2019 results (their Figure 6).

3.4 Ozone Feedback on Northern Hemisphere Jet: Long Response

Interestingly, while the fast responses in the winds and temperatures in the LINOZ ensemble are highly consistent with the results from CP2019, our model also simulates a distinct “long” response characterized by strong cooling over the Arctic from the surface to the mid-to-upper troposphere (Fig. 5b). This cooling, which was not identified in CP2019, results in enhanced mid-to-lower tropospheric temperature gradients, prompting a strong poleward shift of the NH jet and a statistically significant acceleration of the winds at 50°N exceeding 2 m/s (Fig. 5d).

Zonally, the cooling over the Arctic occurring in the LINOZ ensemble during the long response primarily reflects hemispheric-wide cooling over the Arctic associated with an expansion of the North Atlantic Warming Hole (Fig. 6d). This enhancement of meridional temperature gradients in the lower and mid troposphere drives a poleward shift that spans all longitudes and originates over the North Atlantic (Fig. 6b), where the jet exhibits a distinct acceleration and eastward extension over Europe. Note that over the jet core (40-50°N) the winds accelerate (in the zonal mean) during both “fast” (Fig. 5c) and “long” responses (Fig. 5d). However, north of 50°N the responses are very different, with the fast response exhibiting a strong weakening, in contrast to the acceleration occurring on longer (i.e., “long” response) timescales. This behavior north of 50°N was not captured in CP2019 and comprises an ozone feedback that is distinct from what was outlined in that study.

3.5 Long Ozone Feedback: Modulation by the AMOC

The “long” responses in the tropospheric winds and temperatures that occurs in the LINOZ ensemble are not obviously linked to ozone-driven temperature changes in the stratosphere, which do not extend into the troposphere. What, then, is the driver of the lower tropospheric high latitude cooling, if it is not directly linked to ozone-driven stratospheric temperature changes?

As expected from the OMA and NINT results presented in Zhang et al. (Submitted), we find that the strong cooling that occurs over the NH in the long LINOZ response is also related to a weakening of the AMOC at 4xCO₂ (Mitevski et al. (2021); Rind et al. (2020); Orbe et al. (Under Review)). In particular, Figure 7 shows stronger weakening of the AMOC in the LINOZ (green lines) ensemble, relative to NINT (blue lines) at both 26°N (left) and at 48°N (right). Despite large internal variability, the LINOZ ensemble shows a more rapid decline of the AMOC, a difference that is evident at both latitudes.

Interestingly, comparisons of the AMOC behavior in LINOZ with the fully interactive OMA simulation (red line) shows a striking similarity (and the mechanism of these changes is also similar, as shown in Section 3.6). This similarity is surprising, given that other (non-ozone) trace gases and aerosols are also evolving in the OMA experiment. In particular, Rind et al. (2018), using a previous version of the model, observed an indirect effect of natural aerosols (primarily sea salt) on AMOC stability. They showed that aerosols enhanced the local cooling of SSTs in regions of increased cloud cover in a warmer climate by acting as condensation nuclei and thereby raising cloud optical thickness and ocean surface cooling. This surface cooling was then linked to reduced evaporation relative to precipitation, resulting in anomalously positive surface freshwater forcing and reduced North Atlantic Deep Water (NADW) production. That study, however, focused on aerosol-induced AMOC cessations occurring on multicentennial timescales long after the initial (abrupt) warming. By comparison, the results in Figure 7 identify an impact of ozone on the AMOC that occurs within the first 20 years of the initial CO₂ forcing – that is, over the period during which stratospheric temperature gradients are most impacted by ozone (not aerosols). Our results, therefore, highlight that during this time frame the AMOC can be as (if not more) sensitive to wind-driven buoyancy changes forced

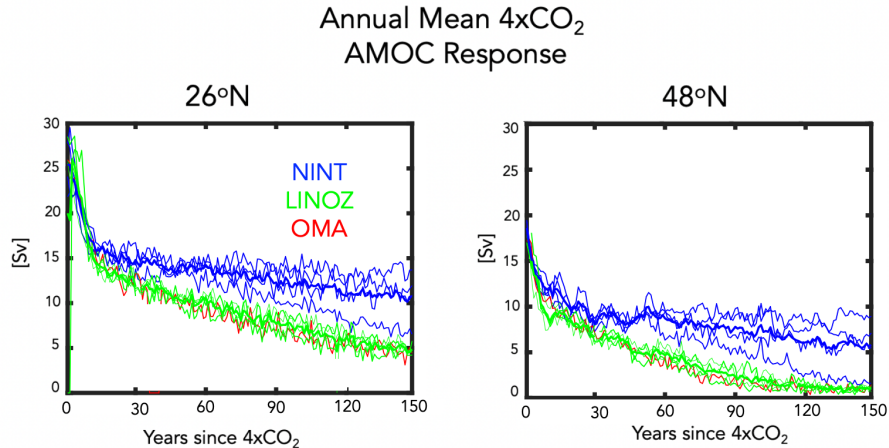


Figure 7. Changes in the annual mean maximum overturning stream function in the Atlantic ocean, evaluated at 26°N (left) and 48°N (right) in response to 4xCO₂, relative to the preindustrial control simulations. Results for the LINOZ and NINT ensembles are shown in green and blue, respectively (thick lines denote ensemble means). Red lines show the response in the OMA simulation.

435 by stratospheric ozone anomalies as they are to aerosol-induced changes in freshwater
436 forcing.

437 Before elucidating the mechanism of the AMOC changes in the LINOZ ensemble,
438 we first identify the region over which the largest differences in mixed layer depth be-
439 gin to emerge between the LINOZ (OMA) and NINT simulations. In particular, the weaker
440 AMOC in the LINOZ and OMA runs is found to be accompanied by a rapid reduction
441 in mixed layer depths, which occur primarily in the Irminger Sea region (55°N–65°N, 40°W–
442 20°W) (Figure 8). The mixed layer depth differences in the Labrador Sea are, by com-
443 parison, negligible. East of the Irminger Sea (i.e., 55°N–65°N, 20°W–0°) we also iden-
444 tify differences between the ensembles (not shown), but these emerge later, suggesting
445 that the Irminger Sea changes are likely the initiators of the differences in AMOC be-
446 havior between the NINT and LINOZ ensembles. A similar region was identified in Romanou
447 et al. (Under Review) as being key for determining the sensitivity of the AMOC, albeit
448 for the low-top model results and SSP 2-4.5 scenario considered in that study.

449 **3.6 Ozone Feedback Dependence on the AMOC: Linking Fast and Long** 450 **Responses**

451 Is the fact that the AMOC declines more rapidly in the LINOZ ensemble – and the
452 OMA run – a response to the ozone changes in those simulations or just a random oc-
453 currence? In the fast response the zonal wind changes over the North Atlantic reflect a
454 weakening of the jet core that is flanked equatorward by positive anomalies, resembling
455 a negative NAO pattern. Indeed, a negative (positive) NAO has been associated with
456 a weaker (stronger) AMOC by adding (extracting) heat to/from the subpolar gyre, re-
457 sulting in reduced (increased) NADW formation (Delworth and Zeng (2016)). Here we
458 argue that such a mechanism is present in our model simulations, resulting in an addi-
459 tional substantial modulation of the NH midlatitude jet location by ozone, this time via
460 its influence on the AMOC.

DJF 4xCO₂ Response in Mixed Layer Depth

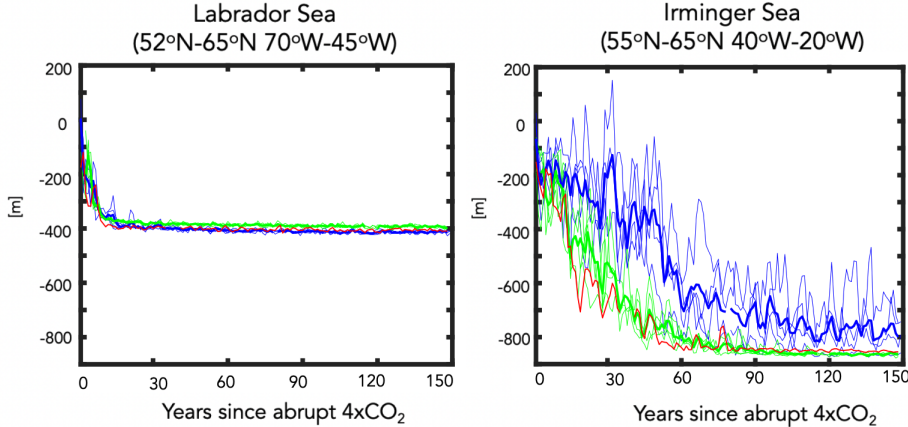


Figure 8. Changes in the DJF mixed layer depths, evaluated over the Labrador Sea (left) and Irminger Sea (right) in response to 4xCO₂, relative to the preindustrial control simulations. Results for the LINOZ and NINT ensembles are shown in green and blue, respectively (thick lines denote ensemble means). Red lines show the response in the OMA simulation.

461 In particular, Figure 9 shows maps of the surface zonal wind, surface friction speed,
 462 mixed layer depth, net heat fluxes, sea surface temperatures, and north-south heat and
 463 salinity ocean transports over years 1-5. In response to an abrupt quadrupling of CO₂,
 464 there is a weak acceleration of the surface zonal winds on the poleward flank of the North
 465 Atlantic jet (~60°N-70°N) (Fig. 9a, top). Over the subpolar North Atlantic the surface
 466 winds weaken, leading to a significant reduction in surface friction speed (Fig. 9b, top)
 467 and mixed layer depths (Fig. 9c, top), as well as increased heat flux into the ocean (in
 468 the form of reduced latent heat fluxes out of the ocean) (Fig. 9d, top) and warmer sea
 469 surface temperatures (Fig. 9e, top). The behavior of the heat fluxes in the subpolar gyre
 470 region is consistent with previous studies showing that a positive (negative) phase of the
 471 NAO implies reduced (enhanced) atmosphere to ocean heat fluxes (Delworth et al., 2017).
 472 At these early years the changes in meridional heat and salinity transports over the Irminger
 473 Sea are relatively small (Fig. 9fg, top).

474 In response to the ozone changes captured in the LINOZ ensemble during years 1-
 475 5, there is a strong reduction in the surface zonal winds and friction speed (Fig. 9 ab,
 476 bottom), consistent with the negative NAO response evident in the 850 hPa zonal winds
 477 (Fig. 6c, top). The surface friction changes align closely with the reduced mixed layer
 478 depths which extend well into the Irminger Sea region and over latitudes further south
 479 of the subpolar gyre (Fig. 9c, bottom).

480 The reductions in mixed layer depth that occur over the Irminger Sea are likely driven
 481 by the reductions in surface wind speed which increased (primarily latent) heat fluxes
 482 into the ocean (Fig. 9d, bottom), driving warmer sea surface temperatures in LINOZ,
 483 relative to NINT (Fig. 9e, bottom). This pattern in heat fluxes is very similar to the NAO
 484 heat flux composites that were prescribed in Delworth and Zeng (2016) and inferred from
 485 observations in Ma et al. (2020), who showed that there is much greater heat loss from
 486 the ocean over the subpolar region in association with a jet strengthening (see their Fig-
 487 ure 6).

488 At the same time, the changes in freshwater forcing (P-E) during this time period
 489 are negligible such that the net buoyancy forcing ($\sim Q+F$) is positive. This stabilizing
 490 buoyancy forcing from surface warming makes the mixed layer depths shallower by sup-
 491 pressing convective mixing, shutting down NADW production (Alexander et al. (2000);
 492 Kantha and Clayson (2000)). There is also an initial change in the north-south heat and
 493 salt transports that is colocated with the dipole anomaly in the surface friction speed,
 494 promoting anomalous poleward salt and heat transport into the subpolar gyre (Fig. 8fg,
 495 bottom). This feature is confined to the top few ocean layers (not shown) and the im-
 496 plied anomalous heat transport could be contributing to the warmer sea surface temper-
 497 atures in that region, in addition to the surface heat flux changes.

498 Over the ensuing years (5-20) a similar pattern is maintained (Figure 10, bottom).
 499 The reduction in NADW, however, results in reduced northward heat and salinity trans-
 500 ports (Fig. 10 fg, middle) throughout the ocean column. While this results in cooler SSTs
 501 south of the subpolar gyre region (Fig. 10e, middle), which otherwise might enhance the
 502 density of the near-surface water masses, the reduced northward salinity transports pre-
 503 vent the AMOC from restarting. Interestingly, the results from the OMA simulation show
 504 a very similar response as the LINOZ ensemble (Figure 10, bottom row), suggesting that
 505 stratospheric ozone changes in that simulation are also the primary driver of the weaker
 506 AMOC in that model configuration. This sequence of processes linking the surface wind
 507 changes to anomalous heat fluxes and reduced NADW is basically identical to what is
 508 outlined in Figure 4 of (Delworth & Zeng, 2016) and Figure 1 of (Khatri et al., 2022).
 509 Additional analysis of the 2xCO₂ simulations, which feature a stronger AMOC decline
 510 in OMA (and LINOZ) compared to NINT (Figure 2), reveals that a similar mechanism
 511 for reduced NADW production occurs at lower CO₂ forcing (not shown).

512 Finally, examining the timescale of the responses of the variables shown in Figures
 513 9 and 10 reinforces the strong coupling between the changes in surface friction speed,
 514 sea surface temperature, latent heat fluxes and mixed layer depth changes over the Irminger
 515 Sea region (Figure 11a-d). Despite large internal variability, there is a clear separation
 516 between the LINOZ (OMA) and NINT simulations that emerges around year 15 (black
 517 dashed lines). The changes in sensible heat emerge after the latent heat fluxes (Fig. 11e),
 518 suggesting that the latter play a more important contribution in initializing the heat flux
 519 differences in LINOZ (OMA), relative to NINT. Furthermore, while they may contribute
 520 to enhanced positive buoyancy forcing later in the integrations, the freshwater forcing
 521 anomalies ($F = P-E$) are shown to be negligible during the initial years following the abrupt
 522 quadrupling of CO₂ (Fig. 11f), indicating that the primary driver of the initial differ-
 523 ence between the LINOZ (OMA) and NINT runs is related to the surface wind-driven
 524 changes as they impact the latent heat fluxes into the ocean. This is consistent with Roach
 525 et al. (2022) who showed a much stronger correlation between AMOC strength at 26°N
 526 and the heat component of the surface buoyancy flux, relative to the freshwater com-
 527 ponent, in various experiments using the Community Earth System Model version 1 (CESM1)
 528 in which the winds over the subpolar gyre were nudged to reanalysis values. Note that
 529 in our model other potential contributors to freshwater forcing from sea ice do reveal dif-
 530 ferences between the LINOZ, OMA and NINT ensembles, but these emerge several years
 531 (i.e., years $\sim 20-30$) after the changes in sea surface temperatures and heat fluxes (not
 532 shown).

533 3.7 Ozone Driver of AMOC Changes: Fixed SST Results

534 So far, we have shown that the stratospheric ozone changes that occur in response
 535 to 4xCO₂ result in a negative NAO response over the North Atlantic (Fig. 5,6). In our
 536 model this triggers a more rapid decline of the AMOC (Fig. 7) through surface-wind driven
 537 changes in heat fluxes into the ocean (Fig. 9,10). While the time series analysis (Fig. 11)
 538 reveals that the AMOC changes in the LINOZ (OMA) ensemble occur on similar timescales
 539 as the wind (and heat flux) changes, one potentially confounding factor is the fact that

DJF 4xCO₂ Response over Years 1-5

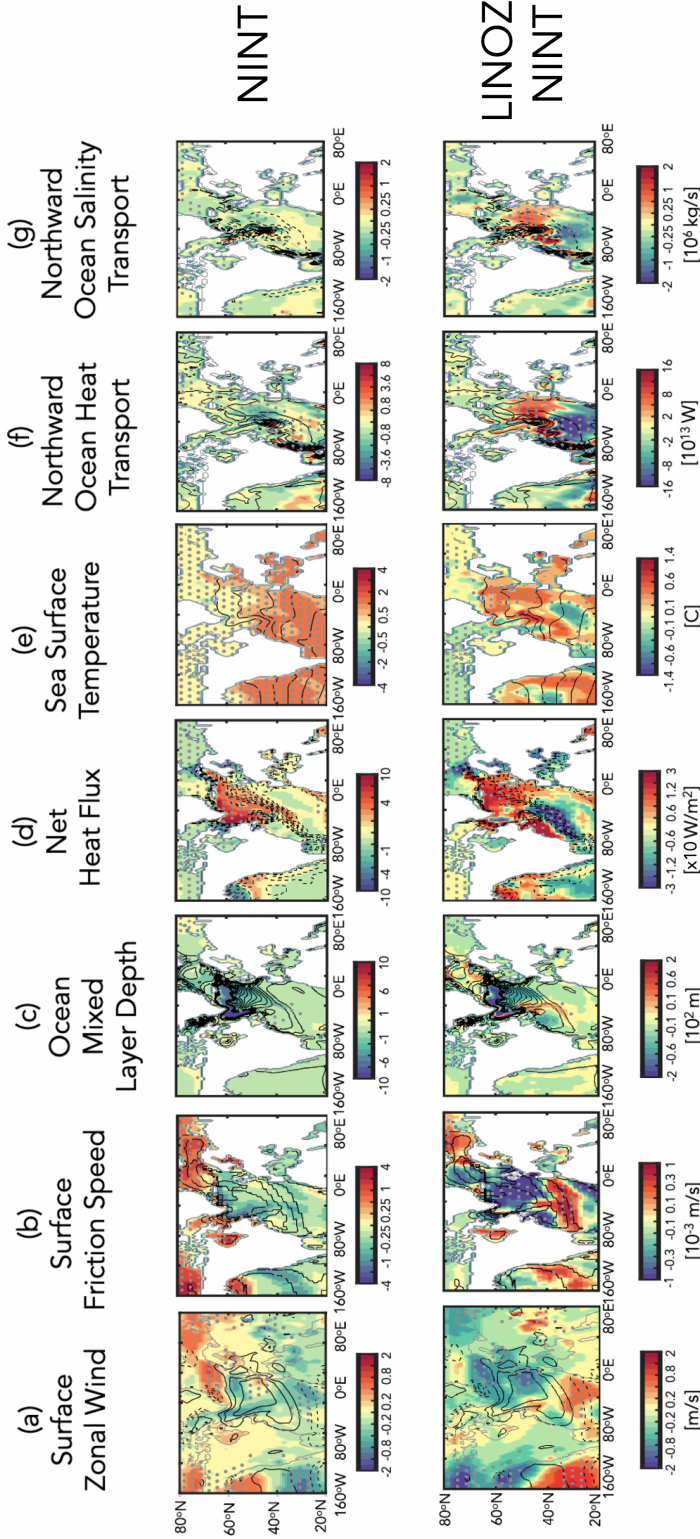


Figure 9. Top panels: Colors show the December-January-February (DJF) response of the surface zonal wind (a), surface friction speed (b), ocean mixed layer depth (c), net heat flux (sum of sensible plus latent heat) (d), sea surface temperature (e) and northward heat (f) and salt (g) transports in response to an abrupt quadrupling of CO₂. Results are shown for the 4-member ensemble averaged NINT configuration. Bottom panels: Same as top panels, except showing the LINOZ minus NINT ensemble mean difference. For both top and bottom panels, responses have been averaged over years 1-5 since “branching” from the preindustrial control simulation. Stippled regions are statistically significant and black contours denote climatological mean DJF values. Contour intervals: surface zonal wind [2 m/s], surface friction speed [2.5x10⁻³ m/s], mixed layer depth [60 m], net heat flux [30 W/m²], sea surface temperature interval [2 C], northward heat flux [2x10¹² W], and northward salt flux [10⁶ kg/s]. The black box in (a) bounds the Irminger Sea region over which the spatial averages in Figure 8b and Figure 11 are evaluated.

DJF 4xCO₂ Response over Years 5-20

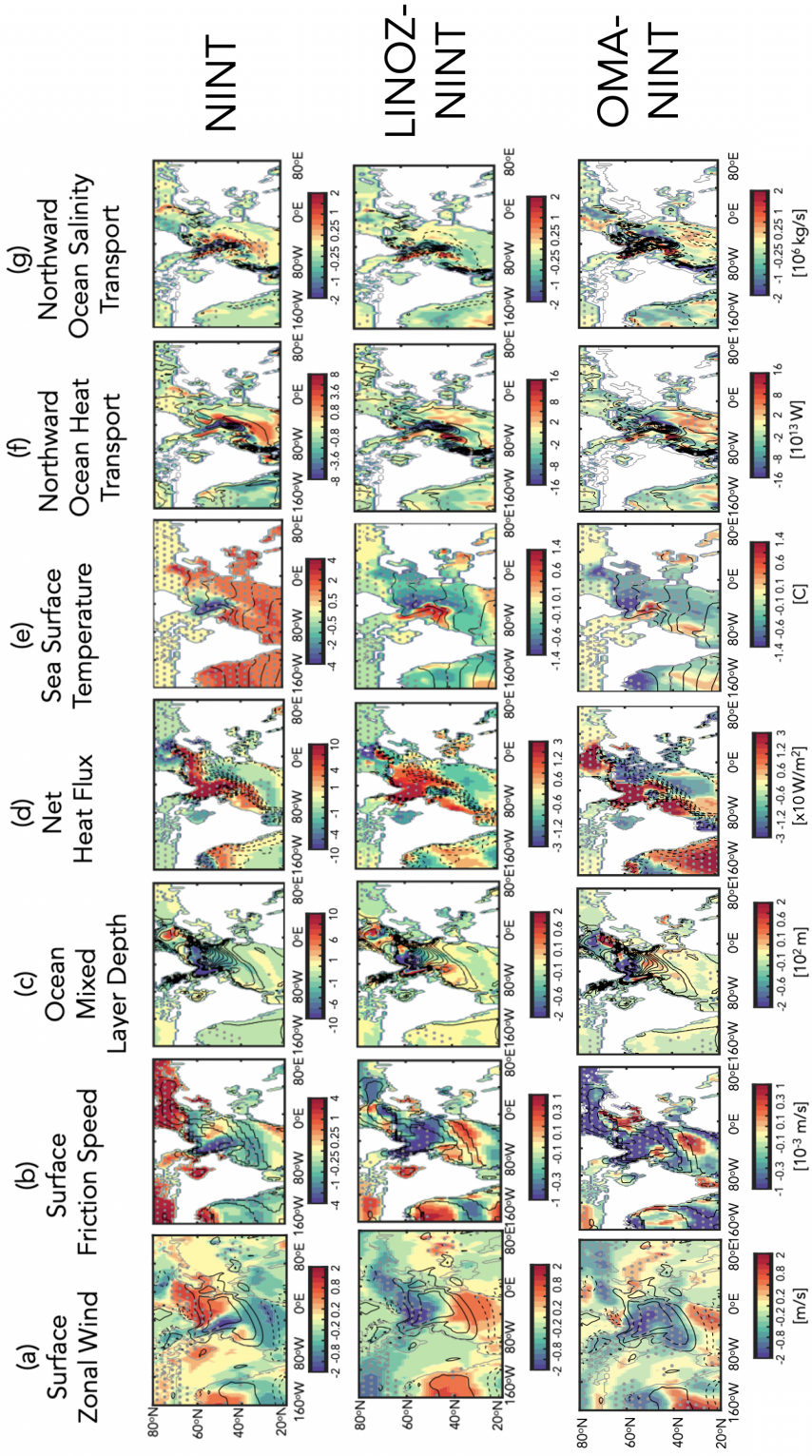


Figure 10. Same as Figure 9, except showing the responses, averaged over years 5-20. An extra row at the bottom has been added, showing the OMA - NINT differences, where the ensemble members shown in Figures 1, 2 and 3 have been used. Same contour intervals and colorbars have been used as in Fig. 9.

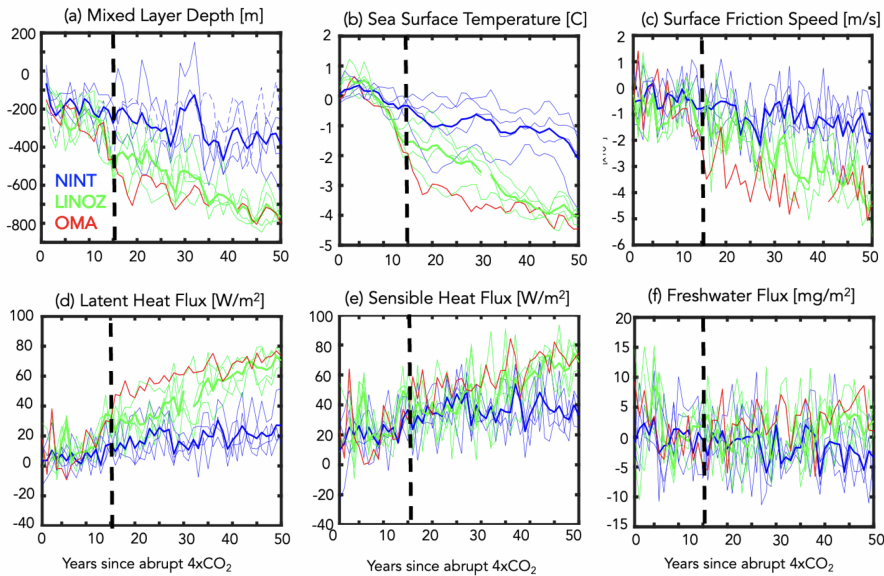
DJF 4xCO₂ Response over Irminger Sea

Figure 11. Changes in the DJF mixed layer depths (a), sea surface temperatures (b), surface friction speed (c), latent heat fluxes (d), sensible heat fluxes (e) and precipitation minus evaporation (f) in response to 4xCO₂, relative to the preindustrial control simulations. Averages are over the Irminger Sea (55°N-65°N, 40°W-20°W). Results for the LINOZ and NINT ensembles are shown in green and blue, respectively (thick lines denote ensemble means). Red lines show the response in the OMA simulation. Black vertical lines indicate year ~15 at which point the mixed layer depth responses in the LINOZ and NINT ensembles diverge. Note that the freshwater flux unit of 1 mg/m² per second ($\equiv 0.0864$ mm/day $\equiv 3.1$ cm/year) is used, because at 5°C it contributes approximately the same ocean density flux as the heat flux unit of 1 W/m² (Large and Yeager (2009)).

540 the AMOC reduction itself results in reduced wind speeds over the subpolar gyre region.
 541 These reduced near-surface winds are associated with an anomalous anticyclonic flow
 542 pattern (Appendix Figure 3, top) (Gervais et al. (2019); Romanou et al. (Under Review);
 543 Orbe et al. (Under Review)), which could contribute to the reduced heat fluxes and sub-
 544 sequent changes in NADW production. Therefore, to more convincingly link the surface
 545 wind speed changes to the stratospheric ozone changes aloft, we next examine results
 546 from the fixed SST experiment.

547 Figure 12 shows the ozone-induced zonal wind and temperature changes averaged
 548 over the last twenty years of the fixed SST and SIC experiments in which the ensemble
 549 mean ozone 4xCO₂ evolution from LINOZ is prescribed (Fig. 12 a,b). Recall that in the
 550 fixed SST experiment, only the ozone evolution differs from the preindustrial control sim-
 551 ulation, as CO₂, SSTs and SIC are all set to preindustrial values. Comparisons with re-
 552 sults from the fully coupled LINOZ “fast” response (see Fig. 5a,c) reveal a very simi-
 553 lar picture. This similarity between the fully coupled fast response and the fixed SST
 554 and SIC experiment is striking, both featuring a similar change in the NH jet associated
 555 with enhanced temperature gradients in the lower stratosphere as first reported in CP2019.

556 Comparisons of the 850 hPa zonal winds and surface temperatures over the North
 557 Atlantic (Fig. 12c,d) also reveal a strikingly similar response between the fully coupled
 558 ensemble and the fixed SST experiment (compare with Fig. 6a,c). Note this similar re-
 559 sponse extends to sea level pressure as well (Appendix Figure 3). This result is inter-
 560 esting as it suggests that over the North Atlantic stratospheric ozone changes alone can
 561 result in a significant reduction in the near surface winds that is on the same order (if
 562 not larger than) the 4xCO₂ response. In our model this additionally results in heat flux
 563 changes that are large enough to reduce NADW production, resulting in a significant (i.e.
 564 30-40%) change in AMOC strength.

565 4 Conclusions

566 Here we have used the NASA GISS coupled atmosphere-ocean high-top model (E2-
 567 2-G) to examine how coupled changes in stratospheric ozone and the ocean circulation
 568 both influence the 4xCO₂ response of the NH midlatitude jet. Our key results are as fol-
 569 lows:

570 1. The NH midlatitude jet response to 4xCO₂ is modulated by coupled feedbacks
 571 from both stratospheric ozone and the AMOC, which occur of “fast” (5-20 year) and “long”
 572 (100-150 year) timescales, respectively.

573 2. In the “fast” response, the zonal mean jet weakens (strengthens) on its poleward
 574 (equatorward) flank, consistent with reduced LS temperature gradients associated with
 575 ozone loss. Zonally, this jet change is expressed as a negative NAO-like pattern, consist-
 576 ing of weaker zonal surface winds over the North Atlantic, consistent with the findings
 577 in CP2019.

578 3. The weaker winds over the North Atlantic are associated with increased (pri-
 579 marily latent) heat fluxes into the ocean which initially result in warmer SSTs over the
 580 subpolar gyre region, reducing NADW production leading to more rapid weakening of
 581 the AMOC.

582 4. A reduced AMOC leads to widespread cooling over the Arctic which enhance
 583 mid-to-lower tropospheric temperature gradients, resulting in a poleward shift of the NH
 584 midlatitude jet. This “long” response is consistent with previous studies showing that
 585 a weakening of the AMOC results in a stronger and poleward shifted jet in the NH (e.g.,
 586 Bellomo et al. (2021); Orbe et al. (Under Review); Liu et al. (2020); Zhang et al. (Sub-
 587 mitted)).

LINOZ – NINT Fixed SST Changes

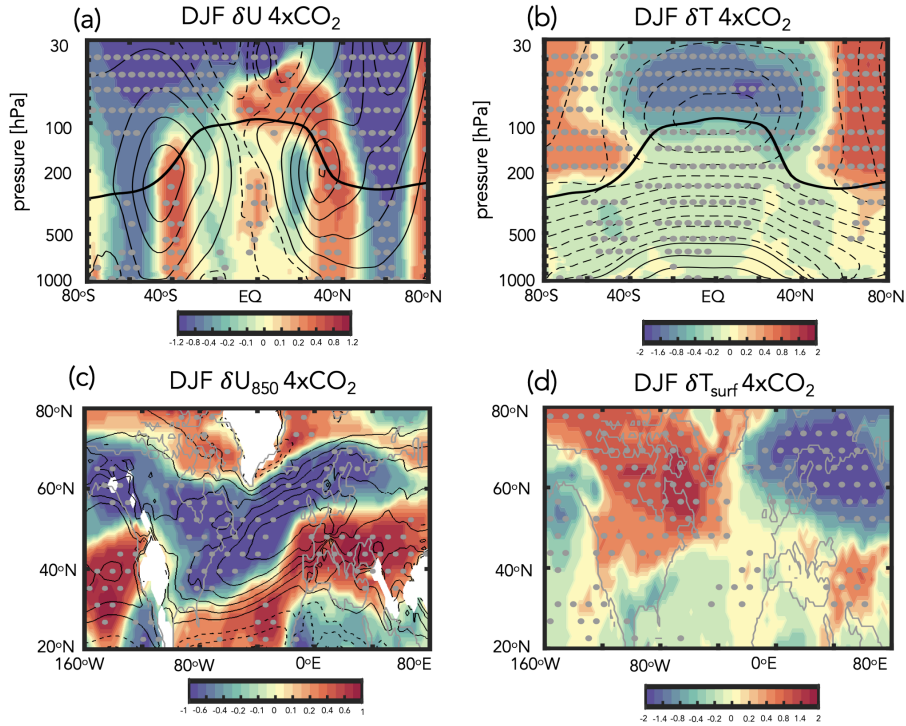


Figure 12. Top panels: Colors show the 4xCO₂ ensemble mean response in zonal mean zonal winds, U (a), temperatures, T (b), 850 hPa zonal winds, U_{850} (c) and surface temperature, T_{surf} (d) in the AMIP experiments in which the time-evolving 4xCO₂ ensemble mean LINOZ ozone response is prescribed. Note that SSTs, SICs and background CO₂ are all set to preindustrial values. Averages are shown over the last 20 years (years 40-60) of the integrations. Black contours, where shown, denote climatological mean DJF values (U contour interval: 8 m/s; T contour interval: 10 K; U_{850} contour interval: 2 m/s). Stippled regions are statistically significant and the black thick line in the top panels shows the climatological mean tropopause in the preindustrial control simulation.

588 Taken together, conclusions 1-4 indicate that the stratospheric ozone feedback on
 589 the NH midlatitude jet reported in CP2019 depends sensitively on the behavior of the
 590 AMOC during the “fast” response, wherein the jet weakens over the North Atlantic. In
 591 our model, this wind response extends to the surface, resulting in reduced heat fluxes
 592 out of the subpolar gyre region and a more rapid decline in the AMOC. On longer timescales,
 593 these changes in the AMOC subsequently drive a poleward shift in the NH midlatitude
 594 jet. While CP2019 identified a jet change mirroring that of the “fast” response documented
 595 here, the “long” response timescale response has not been previously reported, to the
 596 best of our knowledge. This may reflect the fact that many of the stratosphere resolv-
 597 ing chemistry climate models that are used to inform future projections of stratospheric
 598 ozone (Eyring et al. (2008); Fahey et al. (2018)), are not always run coupled to an in-
 599 teractive ocean (Morgenstern et al. (2017)). Among those that are run coupled to a dy-
 600 namic ocean, our results will, of course, need to be tested to assess robustness.

601 Another intriguing result from this study is that the stronger decline of the AMOC
 602 occurring in the LINOZ ensemble does not appear to be a random occurrence. Rather,
 603 in our model, the “fast” ozone and “long” AMOC feedbacks on the NH jet are coupled
 604 through surface-wind driven changes in heat fluxes into the ocean. Key here is the fact
 605 that this sensitivity in the AMOC is driven only by changes in stratospheric ozone, which
 606 we have isolated from changes in other trace gases and aerosols. Thus, while previous
 607 studies (Rind et al. (2018)) have identified an important influence of interactive com-
 608 position on the AMOC, they have mainly implicated the indirect effect of aerosols on
 609 clouds through changes in on sea surface temperatures and how these impact P-E (and
 610 net surface freshwater forcing). To the best of our knowledge, no study has previously
 611 demonstrated an impact of stratospheric ozone changes alone on the AMOC response
 612 to a quadrupling of CO₂. Despite the different mechanisms at play, however, are results
 613 are consistent with those from Rind et al. (2018) in highlighting the need for renewed
 614 focus on surface flux observations to help assess overturning stability.

615 An important caveat with our results is related to known biases in vertical mix-
 616 ing and NADW production in the ocean component of the GISS model (Miller et al. (2021);
 617 Romanou et al. (Under Review)) which likely explain why the low-top version of the cou-
 618 pled atmosphere-ocean climate model (E2-1-G) exhibits a more sensitive AMOC response
 619 to a quadrupling of CO₂, compared to some other models (Bellomo et al. (2021)). At
 620 the same time, the high-top model employed in this study is much less sensitive, as the
 621 AMOC weakens by ~10 SV in response to 4xCO₂, compared to a complete collapse in
 622 E2-1-G (see Figure 31 in Rind et al. (2020)). That study showed that this may be re-
 623 lated to differences in the parameterization of rainfall evaporation associated with moist
 624 convective precipitation, which they show has a strong influence on the AMOC sensi-
 625 tivity in ModelE via its effect on moisture loading in the atmosphere. While an exhaus-
 626 tive comparison between the models is beyond the scope of this study, the relevant point
 627 here is that the 4xCO₂ AMOC response simulated in the E2-2-G NINT ensemble is well
 628 within the CMIP5 and CMIP6 ranges documented in Mitevski et al. (2021) (see their
 629 Supplementary Figure S3).

630 Finally, our results linking the fast timescale jet response to the ensuing AMOC
 631 changes underscore the profound impact that changes in lower stratospheric winds alone
 632 can have on surface climate, as highlighted in Sigmond and Scinocca (2010). Quite re-
 633 markably, our fixed SST and SIC experiment showed that these lower stratospheric wind
 634 changes are driven primarily by changes in ozone and not by background changes in CO₂
 635 or in sea surface boundary conditions. Taken together, our results suggest that more at-
 636 tention needs to be paid to understanding the time-evolving response of the coupled Earth
 637 system to future ozone changes, with a focus on changes in ocean heat transport and how
 638 these feedback on the NH jet stream.

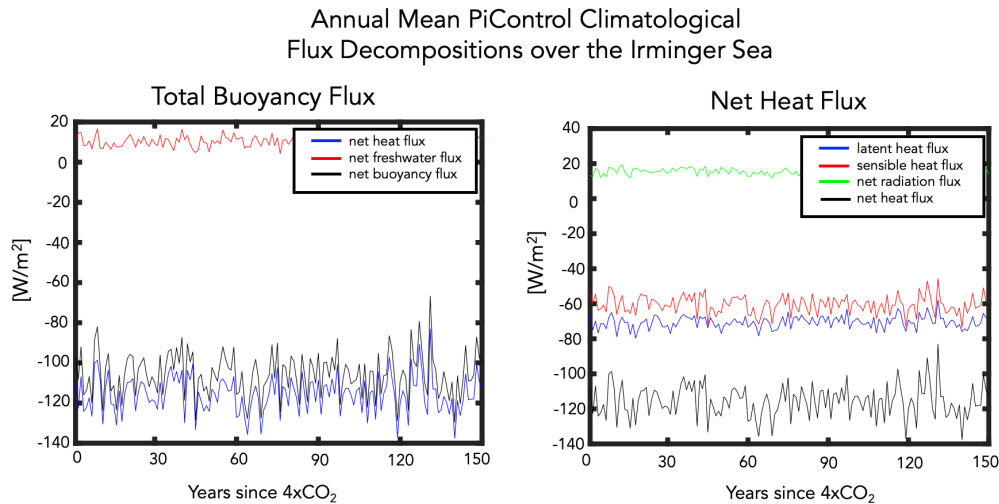


Figure A1. Left: Decomposition of the net surface buoyancy flux (black) into its contributions from net heat (blue) and net freshwater (red) fluxes. Right: Further decomposition of the net surface heat flux (black) into contributions from latent heat fluxes (Q_E (blue)), sensible heat fluxes (Q_H (red)), and combined solar and longwave radiative fluxes (Q_S+Q_L (green)). Results are shown for 150 years of the NINT preindustrial control simulation, evaluated over the Irminger Sea.

639 Appendix A Appendix Figures

640 Open Research Section

641 This section MUST contain a statement that describes where the data supporting
 642 the conclusions can be obtained. Data cannot be listed as "Available from authors" or
 643 stored solely in supporting information. Citations to archived data should be included
 644 in your reference list. Wiley will publish it as a separate section on the paper's page. Ex-
 645 amples and complete information are here: [https://www.agu.org/Publish with AGU/Publish/Author](https://www.agu.org/Publish%20with%20AGU/Publish/Author%20Resources/Data%20for%20Authors)
 646 Resources/Data for Authors

647 Acknowledgments

648 Enter acknowledgments here. This section is to acknowledge funding, thank colleagues,
 649 enter any secondary affiliations, and so on.

650 References

- 651 Alexander, M. A., Scott, J. D., & Deser, C. (2000). Processes that influence sea sur-
 652 face temperature and ocean mixed layer depth variability in a coupled model.
 653 *Journal of Geophysical Research: Oceans*, *105*(C7), 16823–16842.
- 654 Ayarzagüena, B., Charlton-Perez, A. J., Butler, A. H., Hitchcock, P., Simpson, I. R.,
 655 Polvani, L. M., . . . others (2020). Uncertainty in the response of sudden
 656 stratospheric warmings and stratosphere-troposphere coupling to quadrupled
 657 co2 concentrations in cmip6 models. *Journal of Geophysical Research: Atmo-*
 658 *spheres*, *125*(6), e2019JD032345.
- 659 Bauer, S. E., Tsigaridis, K., Faluvegi, G., Kelley, M., Lo, K. K., Miller, R. L., . . .
 660 Wu, J. (2020). Historical (1850–2014) aerosol evolution and role on climate
 661 forcing using the giss modele2. 1 contribution to cmip6. *Journal of Advances*

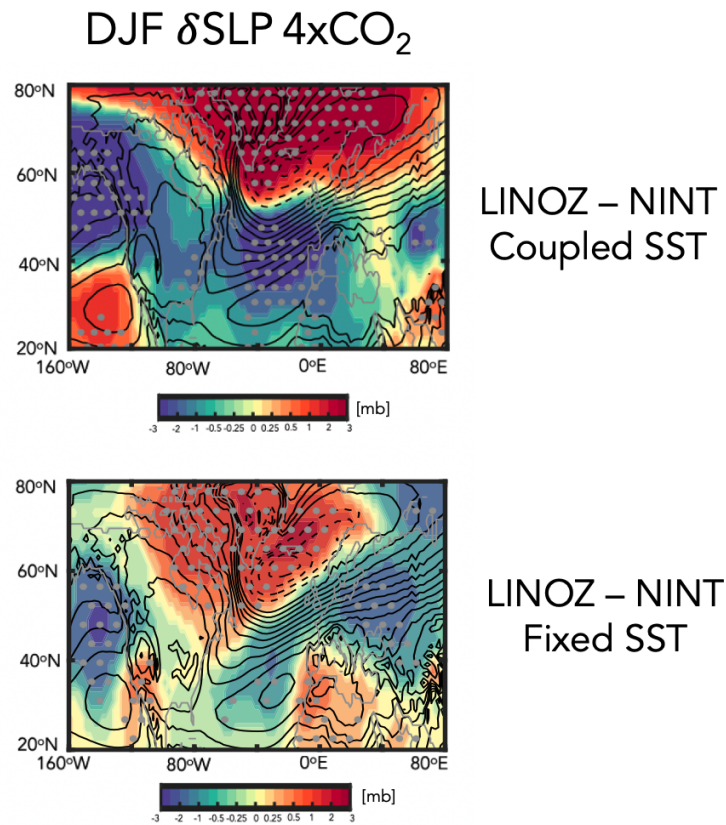


Figure A2. Top panel: Colors show the LINOZ minus NINT ensemble mean difference in the December-January-February (DJF) “fast” response of the sea level pressure in response to an abrupt quadrupling of CO_2 . Results are shown for the fully coupled atmosphere-ocean simulations. Bottom panel: The response in sea level pressure in the AMIP experiments in which the time-evolving $4\times\text{CO}_2$ ensemble mean LINOZ ozone response is prescribed. Note that SSTs, SICs and background CO_2 are set to preindustrial values. Black contours denote climatological mean DJF values (contour interval: 10 mb). Stippled regions are statistically significant.

- 662 *in Modeling Earth Systems*, 12(8), e2019MS001978.
- 663 Bellomo, K., Angeloni, M., Corti, S., & von Hardenberg, J. (2021). Future climate
664 change shaped by inter-model differences in atlantic meridional overturning
665 circulation response. *Nature Communications*, 12(1), 1–10.
- 666 Booth, B. B., Dunstone, N. J., Halloran, P. R., Andrews, T., & Bellouin, N. (2012).
667 Aerosols implicated as a prime driver of twentieth-century north atlantic cli-
668 mate variability. *Nature*, 484(7393), 228–232.
- 669 Butler, A. H., Thompson, D. W., & Heikes, R. (2010). The steady-state atmospheric
670 circulation response to climate change-like thermal forcings in a simple general
671 circulation model. *Journal of Climate*, 23(13), 3474–3496.
- 672 Ceppi, P., & Hartmann, D. L. (2015). Connections between clouds, radiation, and
673 midlatitude dynamics: A review. *Current Climate Change Reports*, 1(2), 94–
674 102.
- 675 Ceppi, P., Zappa, G., Shepherd, T. G., & Gregory, J. M. (2018). Fast and slow com-
676 ponents of the extratropical atmospheric circulation response to co₂ forcing.
677 *Journal of Climate*, 31(3), 1091–1105.
- 678 Chiodo, G., Polvani, L. M., Marsh, D. R., Stenke, A., Ball, W., Rozanov, E., ...
679 Tsigaridis, K. (2018). The response of the ozone layer to quadrupled co₂
680 concentrations. *Journal of Climate*, 31(10), 3893–3907.
- 681 Cowan, T., & Cai, W. (2013). The response of the large-scale ocean circulation
682 to 20th century asian and non-asian aerosols. *Geophysical Research Letters*,
683 40(11), 2761–2767.
- 684 DallaSanta, K., Orbe, C., Rind, D., Nazarenko, L., & Jonas, J. (2021a). Dynamical
685 and trace gas responses of the quasi-biennial oscillation to increased co₂. *Jour-
686 nal of Geophysical Research: Atmospheres*, 126(6), e2020JD034151.
- 687 DallaSanta, K., Orbe, C., Rind, D., Nazarenko, L., & Jonas, J. (2021b). Response of
688 the quasi-biennial oscillation to historical volcanic eruptions. *Geophysical Re-
689 search Letters*, 48(20), e2021GL095412.
- 690 Delworth, T. L., & Dixon, K. W. (2000). Implications of the recent trend in the
691 arctic/north atlantic oscillation for the north atlantic thermohaline circulation.
692 *Journal of Climate*, 13(21), 3721–3727.
- 693 Delworth, T. L., & Zeng, F. (2016). The impact of the north atlantic oscillation on
694 climate through its influence on the atlantic meridional overturning circulation.
695 *Journal of Climate*, 29(3), 941–962.
- 696 Delworth, T. L., Zeng, F., Zhang, L., Zhang, R., Vecchi, G. A., & Yang, X. (2017).
697 The central role of ocean dynamics in connecting the north atlantic oscillation
698 to the extratropical component of the atlantic multidecadal oscillation. *Journal
699 of Climate*, 30(10), 3789–3805.
- 700 Eyring, V., Bony, S., Meehl, G. A., Senior, C. A., Stevens, B., Stouffer, R. J., &
701 Taylor, K. E. (2016). Overview of the coupled model intercomparison project
702 phase 6 (cmip6) experimental design and organization. *Geoscientific Model
703 Development*, 9(5), 1937–1958.
- 704 Eyring, V., Chipperfield, M., Giorgetta, M. A., Kinnison, D. E., Manzini, E.,
705 Matthes, K., ... Waugh, D. W. (2008). Overview of the new ccmval refer-
706 ence and sensitivity simulations in support of upcoming ozone and climate
707 assessments and the planned sparc ccmval report. *SPARC newsletter*, 30,
708 20–26.
- 709 Fahey, D., Newman, P. A., Pyle, J. A., Safari, B., Chipperfield, M. P., Karoly, D.,
710 ... Doherty, S. J. (2018). *Scientific assessment of ozone depletion: 2018, global
711 ozone research and monitoring project-report no. 58*. World Meteorological Or-
712 ganization.
- 713 Garcia, R. R., & Randel, W. J. (2008). Acceleration of the brewer–dobson circula-
714 tion due to increases in greenhouse gases. *Journal of the Atmospheric Sciences*,
715 65(8), 2731–2739.
- 716 Gervais, M., Shaman, J., & Kushnir, Y. (2019). Impacts of the north atlantic warm-

- ing hole in future climate projections: Mean atmospheric circulation and the north atlantic jet. *Journal of Climate*, *32*(10), 2673–2689.
- 717
718
719 Grise, K. M., & Polvani, L. M. (2014). The response of midlatitude jets to increased
720 co2: Distinguishing the roles of sea surface temperature and direct radiative
721 forcing. *Geophysical Research Letters*, *41*(19), 6863–6871.
- 722 Isaksen, I. S., Granier, C., Myhre, G., Berntsen, T., Dalsøren, S. B., Gauss, M., ...
723 others (2009). Atmospheric composition change: Climate–chemistry interac-
724 tions. *Atmospheric Environment*, *43*(33), 5138–5192.
- 725 Kantha, L. H., & Clayson, C. A. (2000). *Small scale processes in geophysical fluid*
726 *flows*. Elsevier.
- 727 Khatri, H., Williams, R. G., Woollings, T., & Smith, D. M. (2022). Fast and slow
728 subpolar ocean responses to the north atlantic oscillation: Thermal and dy-
729 namical changes. *Geophysical Research Letters*, *49*(24), e2022GL101480.
- 730 Lindzen, R. S. (1987). On the development of the theory of the qbo. *Bulletin of the*
731 *American Meteorological Society*, 329–337.
- 732 Liu, W., Fedorov, A. V., Xie, S.-P., & Hu, S. (2020). Climate impacts of a weak-
733 ened atlantic meridional overturning circulation in a warming climate. *Science*
734 *advances*, *6*(26), eaaz4876.
- 735 Ma, L., Woollings, T., Williams, R. G., Smith, D., & Dunstone, N. (2020). How
736 does the winter jet stream affect surface temperature, heat flux, and sea ice in
737 the north atlantic? *Journal of Climate*, *33*(9), 3711–3730.
- 738 Marsh, D. R., Lamarque, J.-F., Conley, A. J., & Polvani, L. M. (2016). Strato-
739 spheric ozone chemistry feedbacks are not critical for the determination of
740 climate sensitivity in cesm1 (waccm). *Geophysical Research Letters*, *43*(8),
741 3928–3934.
- 742 Marshall, J., Johnson, H., & Goodman, J. (2001). A study of the interaction of
743 the north atlantic oscillation with ocean circulation. *Journal of Climate*, *14*(7),
744 1399–1421.
- 745 McLinden, C., Olsen, S., Hannegan, B., Wild, O., Prather, M., & Sundet, J.
746 (2000). Stratospheric ozone in 3-d models: A simple chemistry and the cross-
747 tropopause flux. *Journal of Geophysical Research: Atmospheres*, *105*(D11),
748 14653–14665.
- 749 Miller, R. L., Schmidt, G. A., Nazarenko, L. S., Bauer, S. E., Kelley, M., Ruedy, R.,
750 ... others (2021). Cmp6 historical simulations (1850–2014) with giss-e2. 1.
751 *Journal of Advances in Modeling Earth Systems*, *13*(1), e2019MS002034.
- 752 Mitevski, I., Orbe, C., Chemke, R., Nazarenko, L., & Polvani, L. M. (2021). Non-
753 monotonic response of the climate system to abrupt co2 forcing. *Geophysical*
754 *research letters*, *48*(6), e2020GL090861.
- 755 Morgenstern, O., Hegglin, M. I., Rozanov, E., O’Connor, F. M., Abraham, N. L.,
756 Akiyoshi, H., ... others (2017). Review of the global models used within
757 phase 1 of the chemistry–climate model initiative (ccmi). *Geoscientific Model*
758 *Development*, *10*(2), 639–671.
- 759 Nowack, P. J., Luke Abraham, N., Maycock, A. C., Braesicke, P., Gregory, J. M.,
760 Joshi, M. M., ... Pyle, J. A. (2015). A large ozone-circulation feedback and
761 its implications for global warming assessments. *Nature climate change*, *5*(1),
762 41–45.
- 763 O’Callaghan, M. J. D. S., Ameen, & Mitchell, D. (2014). The effects of different sud-
764 den stratospheric warming types on the ocean. *Geophysical Research Letters*,
765 *41*(21), 7739–7745.
- 766 Orbe, C., Rind, D., Jonas, J., Nazarenko, L., Faluvegi, G., Murray, L. T., ... oth-
767 ers (2020). Giss model e2. 2: A climate model optimized for the middle
768 atmosphere—2. validation of large-scale transport and evaluation of cli-
769 mate response. *Journal of Geophysical Research: Atmospheres*, *125*(24),
770 e2020JD033151.
- 771 Orbe, C., Rind, D., Miller, R., Nazarenko, L., Romanou, A., Jonas, J., ... Schmidt,

- 772 G. (Under Review). Atmospheric response to a collapse of the north atlantic
773 circulation under a mid-range future climate scenario: A regime shift in north-
774 ern hemisphere dynamics. *Journal of Climate*.
- 775 Reichler, T., Kim, J., Manzini, E., & Kröger, J. (2012). A stratospheric connection
776 to atlantic climate variability. *Nature Geoscience*, *5*(11), 783–787.
- 777 Rind, D., Jonas, J., Balachandran, N., Schmidt, G. A., & Lean, J. (2014). The
778 qbo in two giss global climate models: 1. generation of the qbo. *Journal of*
779 *Geophysical Research: Atmospheres*, *119*(14), 8798–8824.
- 780 Rind, D., Orbe, C., Jonas, J., Nazarenko, L., Zhou, T., Kelley, M., ... others
781 (2020). Giss model e2. 2: A climate model optimized for the middle atmo-
782 sphere—model structure, climatology, variability, and climate sensitivity.
783 *Journal of Geophysical Research: Atmospheres*, *125*(10), e2019JD032204.
- 784 Rind, D., Schmidt, G. A., Jonas, J., Miller, R., Nazarenko, L., Kelley, M., & Roman-
785 ski, J. (2018). Multicentury instability of the atlantic meridional circulation in
786 rapid warming simulations with giss modele2. *Journal of Geophysical Research:*
787 *Atmospheres*, *123*(12), 6331–6355.
- 788 Rind, D., Suozzo, R., Balachandran, N., Lacis, A., & Russell, G. (1988). The giss
789 global climate-middle atmosphere model. part i: Model structure and climatol-
790 ogy. *Journal of the atmospheric sciences*, *45*(3), 329–370.
- 791 Roach, L. A., Blanchard-Wrigglesworth, E., Ragen, S., Cheng, W., Armour, K. C.,
792 & Bitz, C. M. (2022). The impact of winds on amoc in a fully-coupled climate
793 model. *Geophysical Research Letters*, e2022GL101203.
- 794 Romanou, A., Rind, D., Jonas, J., Miller, R., Kelley, M., Russel, G., ... Schmidt,
795 G. A. (Under Review). Stochastic bifurcation of the North Atlantic circula-
796 tion under a mid-range future climate scenario with the NASA-GISS ModelE.
797 *Journal of Climate*.
- 798 Shaw, T., Baldwin, M., Barnes, E. A., Caballero, R., Garfinkel, C., Hwang, Y.-T.,
799 ... others (2016). Storm track processes and the opposing influences of climate
800 change. *Nature Geoscience*, *9*(9), 656–664.
- 801 Shaw, T. A. (2019). Mechanisms of future predicted changes in the zonal mean mid-
802 latitude circulation. *Current Climate Change Reports*, *5*(4), 345–357.
- 803 Shepherd, T. G. (2014). Atmospheric circulation as a source of uncertainty in cli-
804 mate change projections. *Nature Geoscience*, *7*(10), 703–708.
- 805 Sigmond, M., & Scinocca, J. F. (2010). The influence of the basic state on the
806 northern hemisphere circulation response to climate change. *Journal of Cli-*
807 *mate*, *23*(6), 1434–1446.
- 808 Simpson, I. R., Shaw, T. A., & Seager, R. (2014). A diagnosis of the seasonally
809 and longitudinally varying midlatitude circulation response to global warming.
810 *Journal of the Atmospheric Sciences*, *71*(7), 2489–2515.
- 811 Smith, D. M., Screen, J. A., Deser, C., Cohen, J., Fyfe, J. C., García-Serrano, J.,
812 ... others (2019). The polar amplification model intercomparison project
813 (pamip) contribution to cmip6: investigating the causes and consequences of
814 polar amplification. *Geoscientific Model Development*, *12*(3), 1139–1164.
- 815 Swingedouw, D., Ortega, P., Mignot, J., Guilyardi, E., Masson-Delmotte, V., But-
816 tler, P. G., ... Sférian, R. (2015). Bidecadal north atlantic ocean circulation
817 variability controlled by timing of volcanic eruptions. *Nature communications*,
818 *6*(1), 1–12.
- 819 Vallis, G. K., Zurita-Gotor, P., Cairns, C., & Kidston, J. (2015). Response of the
820 large-scale structure of the atmosphere to global warming. *Quarterly Journal*
821 *of the Royal Meteorological Society*, *141*(690), 1479–1501.
- 822 Visbeck, M., Cullen, H., Krahmman, G., & Naik, N. (1998). An ocean model’s re-
823 sponse to north atlantic oscillation-like wind forcing. *Geophysical research let-*
824 *ters*, *25*(24), 4521–4524.
- 825 Voigt, A., & Shaw, T. A. (2015). Circulation response to warming shaped by radia-
826 tive changes of clouds and water vapour. *Nature Geoscience*, *8*(2), 102–106.

- 827 Yuval, J., & Kaspi, Y. (2020). Eddy activity response to global warming-like tem-
828 perature changes. *Journal of Climate*, *33*(4), 1381–1404.
- 829 Zhai, H. L. J., Xiaoming, & Marshall, D. P. (2014). A simple model of the response
830 of the atlantic to the north atlantic oscillation. *Journal of Climate*, *27*(11),
831 4052–4069.
- 832 Zhang, X., Waugh, D., & Orbe, C. (Submitted). Response of Tropospheric Ttrans-
833 port to Abrupt CO2 Increase: D]ependence on the Atlantic Meridional Over-
834 turning Circulation. *Journal of Geophysical Research: Atmospheres*.